Renewable Energy 92 (2016) 192–201

Contents lists available at ScienceDirect

Renewable Energy

journal homepage: www.elsevier.com/locate/renene

Performance validation and optimization of a dual coaxial-cylinder ocean-wave energy extractor

Daewoong Son, Valentin Belissen [1], Ronald W. Yeung [*]

Department of Mechanical Engineering, University of California at Berkeley, Berkeley, CA 94720, USA

ARTICLE INFO

Article history:
Received 3 August 2015
Received in revised form
28 December 2015
Accepted 6 January 2016
Available online xxx

Keywords:
Ocean-wave energy
Wave-energy extractor
Coaxial cylinders
Optimization
Motion amplification
Permanent-magnet linear generator

ABSTRACT

A point-absorber wave-energy extractor is developed, consisting of a dual coaxial-cylinder system, with the inner cylinder tension-tethered and an outer cylinder (floater) oscillating vertically. A permanent magnet linear generator (PMLG) is used as a power take-off (PTO) capturing wave energy from the relative motion of the two cylinders. The mathematical modeling of the system includes the coupling effects of the cylinder hydrodynamics and the PMLG behavior. It gives a rational and effective way of providing performance predictions and directions for optimization. The flat bottom shape of the floater is modified into a needle-like curved shape to minimize viscous losses, which leads to three-times increase in floater response, compared with the flat-bottom geometry and thus improved wave-energy capture. The behavior of the PTO in the presence of an appropriate supporting structure for the coaxial cylinders are investigated, and optimal operating conditions for energy extraction and mechanical to electrical conversion efficiency are determined. Experimental results of this coupled system in regular waves confirm the validity of the theoretical predictions and soundness of the engineering design. Optimizing the floater bottom shape and the operating conditions for energy extraction lead to a two-times increase in overall efficiency, even without any active control.

1. Introduction

Because of the growth of the world energy demand, research on renewable energy utilization is important. According to the International Energy Outlook 2011 by the U.S. Energy Information Administration, the energy consumption of the world will grow by more than 50% from 2008 to 2035 [1]. Furthermore, there is no doubt that the use of fossil fuels causes serious environmental and climate issues. Ocean waves thus is one of the promising renewable energy alternatives because of the highest energy density compared to others, such as solar and wind. In fact, the worldwide potential of wave-energy is estimated about 2 TW [2], which is the same order of current world annual electricity consumption rate.

In contrast to other renewable sources, a wide variety of concepts for wave-energy extractor are being examined [3,4]. In this work, a dual coaxial-cylinder system of a point-absorber type device is designed and fabricated so that it is operable without mounting to any fixed platform in the open ocean. The inner cylinder is tension-tethered to the seabed or moored, while the outer cylinder of toroidal shape floats and slides freely in the vertical direction. This axisymmetric point-absorber device can be set in resonance with the incident waves and is insensitive to the incoming-wave direction. Analytical solutions of the radiation problem for the coaxial cylinders and the wave-exciting forces were recently developed [5], which allows the prediction of the floater response in frequency domain.

The most similar two-body heaving devices to this research can be found in L10 Buoy of Oregon State University [6], PowerBuoy of Ocean Power Technology [7], and Wavebob [8]. Typically, an outer body of such two-body devices have designs that are of very high radius-draft ratio. The design proposed here with a low radius-draft ratio was chosen to fit our experimental facility for ease of validation of the theoretical model. This lower radius-draft ratio, that is a deeper draft and smaller radius, leads to larger energy extraction capabilities [9]. The approach and analysis can be applied to any geometric proportions with little difficulty.

This kind of two-body heaving device, which is compact and "self-contained", extracts the wave-energy by the relative heave

* Corresponding author. Marine Mechanics Laboratory (MML), University of California at Berkeley, USA.
E-mail addresses: dwoong.son@berkeley.edu (D. Son), v.belissen@gmail.com (V. Belissen), rwyeung@berkeley.edu (R.W. Yeung).
[1] Current address: Nenuphar Wind, 59000 Lille, France.

http://dx.doi.org/10.1016/j.renene.2016.01.032
0960-1481/

motion using an installed power take-off (PTO) system between the two bodies. A direct-drive conversion system would be highly superior to any moving mechanical parts involving gearing and hydraulics. For this purpose, a permanent magnet linear generator (PMLG) is being used, which includes a translator of a magnet array and a stator with coils. This PMLG for this work was specially designed and studied in the authors' research laboratory [10,11]. The generator damping highly affects the power extraction and the overall system behavior. Thus, an appropriate generator damping must be chosen to increase the instantaneous power output.

In addition to the generator damping, fluid viscosity has important effect on the motion of the floating body. In particular, it was found that the bottom shape of the floater plays an important part in the hydrodynamic coefficients, especially damping, which is strongly related to the body motion [12]. A specially chosen profiled bottom shape of the floater following the design of "The Berkeley Wedge" [13] led to increased motion response at resonance compared to that of a flat bottom, which can be explained by a reduction of the flow separation and the vorticity generation from the body.

This paper describes the design and fabrication of the dual cylinder system as a "stand-alone" working physical unit and the customization of the PMLG unit suitable for the floating system. It will demonstrate the viability of the concept and effectiveness of the prediction from the developed theoretical model. Furthermore, improvements of the system to enhance the performance will be explained. Finally, the system will be examined to find optimal operating conditions and to determine to what extent the performance improvements are achieved.

2. Theoretical modeling of the coupled system

Assuming that the fluid is inviscid and incompressible, and the flow is irrotational, we can use linear-wave theory with the inclusion of the effects of the PTO as an external force. This section reviews the formulation for modeling the interaction between incident waves and the floating point absorber [9–11,14,15], the solution for the latter's motion is a requisite for this energy extraction.

2.1. Floater hydrodynamics

The schematic of the two coaxial, vertical-cylinders absorber system is illustrated in Fig. 1. The cylinders experience surge $\zeta_1(t)$, heave $\zeta_3(t)$, and pitch $\zeta_5(t)$ motion. The incident wave propagating along the x-direction is described by elevation $\eta(x,t)$; and the periodic motions of the body $\zeta_i(t)$ are defined by:

$$\eta(x,t) = \Re\left\{Ae^{i(kx-\sigma t)}\right\} \tag{1}$$

$$\zeta_i(t) = \Re\left\{\mathscr{A}_i e^{-i\sigma t}\right\} \tag{2}$$

where A is the incident-wave amplitude, k is the wave number, σ is the angular frequency, and $\mathscr{A}_i$ is the complex amplitude of the floater motion in the i-direction.

Per linear theory, this dual coaxial-cylinder system behaves as a single body in the surge ($i=1$) and the pitch motion ($i=5$), whereas each cylinder has independent heave motion ($i=3$), decoupled from the surge and pitch modes [9]. Furthermore, in our design, the inner cylinder is considered to be relatively fixed. Thus, the equation of heave motion for the outer cylinder induced by the incident-waves can be written as:

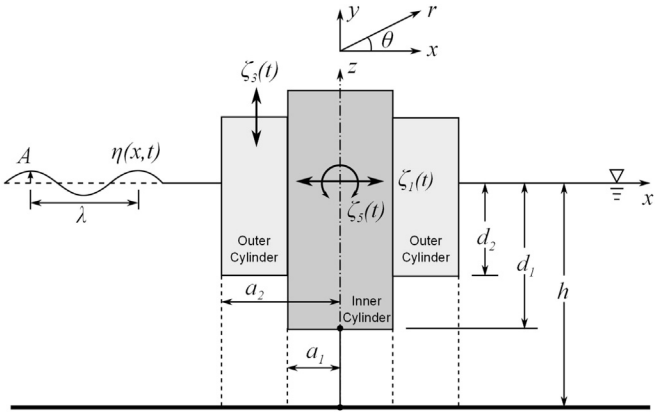

Fig. 1. Schematic of the two coaxial-cylinder system.

$$(m_2+\mu_{33})\ddot{\zeta}_3(t) + \lambda_{33}\dot{\zeta}_3(t) + K_{33}\zeta_3(t) = AX_3e^{-i\sigma t} \tag{3}$$

where $m_2,\mu_{33},\lambda_{33},K_{33},X_3$ are the displaced mass, added mass, inviscid radiation damping, spring constant of the outer cylinder, and complex wave-exciting force amplitude, respectively. The hydrodynamic quantities, added mass μ_{33}, inviscid radiation damping λ_{33}, and complex wave-exciting force amplitude X_3 can be computed by integrating appropriate potentials over the wetted surface:

$$\mu_{33} + \frac{\lambda_{33}}{-i\sigma} = \rho\int_{S_B}\phi_3 n_3 dS \tag{4}$$

$$X_3 = |X_3|e^{i\delta_3} = i\rho\sigma\int_{S_B}[\phi_0+\phi_7]n_3 dS \tag{5}$$

where $\rho,\phi_0,\phi_3,\phi_7,n_3,S_B$ are the water density, the spatial potential of the incident-wave, the radiation in heave, the diffraction potential, the unit normal into the body surface in vertical direction, and the wetted surface, respectively. Here, the fluid flow, described by the spatial potential $\phi_i, i=0,3,7$ using the linear-wave theory, must satisfy the Laplace equation in the fluid domain and the free-surface, seabed, body, and radiation boundary conditions. The frequency-dependent added mass, radiation damping, and wave-exciting force were obtained from Ref. [5] for a given set geometric proportions, Fig. 2, with variable definition recalled from this reference.

In a real fluid, viscous effects are present. Thus, the total hydrodynamic damping λ_T of the floater is introduced to include the viscous (equivalent linearized) damping λ_{vis} to represent such additional effects:

$$\lambda_T = \lambda_{33} + \lambda_{vis} = f_{vis}\lambda_{33}, \quad \text{with } f_{vis} \equiv \frac{\lambda_T}{\lambda_{33}} \tag{6}$$

The heave motion response, Eqn. (3), in non-dimensional form for the floater relative to the incident-wave amplitude, i.e., the response-amplitude operator (RAO), with the use of Eqns. (1), (2) and (6) is given by:

$$\left|\frac{\mathscr{A}_3}{A}\right| = \frac{|\overline{X}_3|}{\sqrt{\left[\gamma-\overline{\sigma}^2(\overline{m}_2+\overline{\mu}_{33})\right]^2+\left[\overline{\sigma}^2\overline{\lambda}_T\right]^2}} \tag{7}$$

where $\overline{X}_3 = X_3/\pi\rho g a_2^2, \gamma = 1-(a_{2,in}/a_2)^2, \overline{\sigma}^2 = \sigma^2 a_2/g, \overline{m}_2 = m_2/\pi\rho a_2^3, \overline{\mu}_{33} = \mu_{33}/\pi\rho a_2^3, \overline{\lambda}_T = \lambda_T/\pi\rho\sigma a_2^3$. From the above expression, the

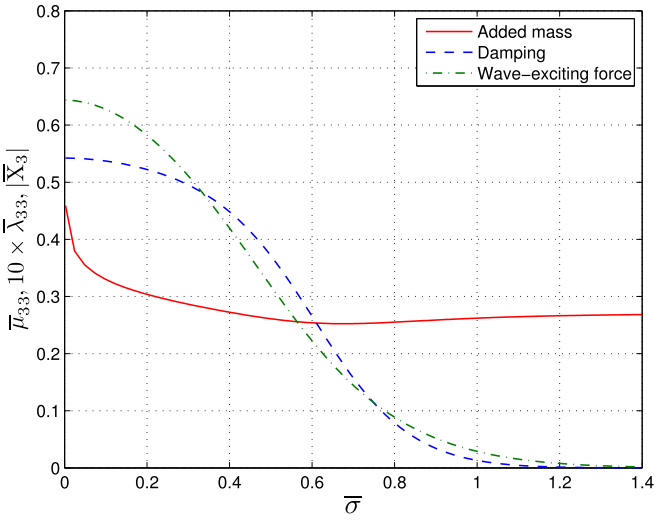

Fig. 2. Non-dimensional hydrodynamic coefficients obtained from Ref. [5] for given geometric properties, see Table 1.

floater response can be maximized at the following so-called "resonance condition":

$$\overline{\sigma}_{res} = \sqrt{\frac{\gamma}{[\overline{m}_2 + \overline{\mu}_{33}(\overline{\sigma}_{res})]}} \tag{8}$$

where an implicit knowledge of the added mass is required.

2.2. Modeling of the coupled system

Fully coupling analysis in the presence the linear generator is important to predict the power capture from waves. When the linear generator is attached to wave-energy extractor system, an additional external electro-magnetic force $F_g(t)$ will oppose to the direction of the moving translator, with the dominant contribution term defined as in Ref. [10]:

$$F_g(t) = -B_g\dot{\zeta}_3(t) \tag{9}$$

where B_g is the force coefficient of the generator as a damper. As pointed out in Ref. [10], inertia effects were minimal. The RAO expression of the floater coupled with the linear generator becomes:

$$\left|\frac{\mathscr{X}_3}{A}\right| = \frac{|\overline{X}_3|}{\sqrt{\left[\gamma - \overline{\sigma}^2(\overline{m}_2 + \overline{\mu}_{33})\right]^2 + \left[\overline{\sigma}^2\overline{\lambda}_T\left(1+\tilde{f}\right)\right]^2}} \tag{10}$$

Here, $\tilde{f}$ is introduced to express the generator damping to the total hydrodynamic damping of the fluid of the floater:

$$\tilde{f} \equiv \frac{B_g}{\lambda_T} \tag{11}$$

2.3. Power extraction and energy-capture width

The time-averaged rate of work done $\overline{\dot{W}}$ over one period T, or mechanical power going into the generator, can be expressed as: after some an integration step.

$$\overline{\dot{W}} = \frac{1}{T}\int_{t-T/2}^{t+T/2} B_g\dot{\zeta}_3^2(t)dt = \frac{\pi}{2}\rho(ga_2)^{\frac{3}{2}}|\mathscr{X}_3|^2\overline{\sigma}^3\tilde{f}\ \overline{\lambda}_T \tag{12}$$

When combined with the RAO expression, Eqn. (10), the time-averaged mechanical power per wave-amplitude squared A^2 at the resonance frequency becomes:

$$\left.\frac{\overline{\dot{W}}}{A^2}\right|_{res} = \frac{\pi}{2}\rho(ga_2)^{\frac{3}{2}}\frac{|\overline{X}_3|^2}{\overline{\sigma}_{res}\overline{\lambda}_T}\frac{\tilde{f}}{\left(1+\tilde{f}\right)^2} \tag{13}$$

Straight-forward differentiation of the above with respect to $\tilde{f}$ allows us to deduce that the optimal generator damping coefficient is equal to the total hydrodynamic damping, i.e., $B_g{=}\lambda_T$, or $\tilde{f}=1$. This leads to the maximized time-averaged mechanical power at resonance:

$$\left.\frac{\overline{\dot{W}}}{A^2}\right|_{max} = \frac{\pi}{8}\rho(ga_2)^{\frac{3}{2}}\frac{|\overline{X}_3|^2}{\overline{\sigma}_{res}\overline{\lambda}_T} \tag{14}$$

Meanwhile, the wave energy flux incident on the floater per unit wave front in deep water is given by:

$$P_{wave} = \frac{1}{2}\rho g A^2 V_g = \frac{1}{8\pi}\rho g^2 A^2 T \tag{15}$$

where V_g is the group velocity for deep water. In terms of wave-energy extraction efficiency, a capture width C_w is used which is the effective width of incident-waves from which the energy is extracted. The capture width at the resonance is hence given by:

$$C_w = \frac{\overline{\dot{W}}}{P_{wave}} = \frac{1}{k_{res}}\left[\frac{\pi\overline{\sigma}^2|\overline{X}_3|^2}{2\overline{\lambda}_{33}}\right]\frac{1}{f_{vis}}\eta_{me} \tag{16}$$

where η_{me} is mechanical efficiency factor:

$$\eta_{me} = \frac{4\tilde{f}}{\left(1+\tilde{f}\right)^2} \tag{17}$$

This capture width expression, Eqn. (16), allows one to identify several important facts in the absorber design:

1. The mechanical efficiency η_{me} can be maximized by tuning the generator damping B_g to the total hydrodynamic damping λ_T, i.e. $\tilde{f}=1$ at resonance frequency. Fortunately η_{me} does not turn out to be very narrow peaked.
2. If the Haskind's relation [16] is used, which is a reciprocity relationship between the wave-exciting force and radiation damping, the bracket term becomes unity.
3. If the fluid were inviscid, $f_{vis}=1$, and the above two items are true, then the well-known inviscid-fluid result is recovered: $k_{res}C_w=1$.
4. In a viscous fluid, the capture width C_w is reduced by the viscous factor of $1/f_{vis}$; the reduction of f_{vis} is seen to be important.

The above discussion does not take into account the mechanical work to electrical energy conversion may not be 100% as the PTO is not perfect. If the energy is dissipated through the resistor of impedance R with a current of intensity $i(t)$ and a voltage drop across the resistor $v(t)$, the time-averaged electrical power output is:

$$P_{el} = \frac{1}{T}\int_{t-T/2}^{t+T/2}\frac{v^2(t)}{R}\,dt = \frac{1}{T}\int_{t-T/2}^{t+T/2}Ri^2(t)\,dt \tag{18}$$

Thus, the useful power output will depend on the mechanical-

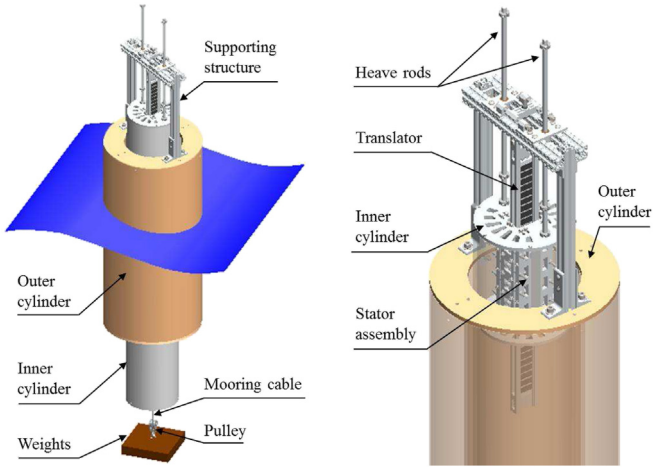

Fig. 3. Overview of the developed dual coaxial-cylinder system.

Table 1
Geometric parameters of the model.

Inner cylinder radius	a_1	[m]	0.137
Inner cylinder length	l_1	[m]	1.803
Inner cylinder draft	d_1	[m]	1.067
Outer cylinder inside radius	$a_{2,in}$	[m]	0.151
Outer cylinder outside radius	a_2	[m]	0.254
Outer cylinder length	l_2	[m]	1.067
Outer cylinder draft	d_2	[m]	0.635
Water depth	h	[m]	1.500
Non-dim. target resonance frequency	$\overline{\sigma}_{res}$	–	0.583
Target resonance wave period	T_{res}	[s]	1.735

electrical energy conversion efficiency η_{el} of PTO, that is:

$$\eta_{el} = \frac{P_{el}}{P_{me}} = \frac{P_{el}}{\dot{W}} \tag{19}$$

In summary, the *effective* capture width $C_{w|out}$, including the conversion efficiency and with the use of the Haskind's relation, will be:

$$C_{w|out} = \eta_{el} C_w = \frac{1}{k_{res}} \frac{1}{f_{vis}} \eta_{el} \eta_{me} \tag{20}$$

Eqn. (20) provides clear directions to increase the effective capture width:

1. Decrease λ_T to increase the floater motion response.
2. Match the generator damping B_g to achieve $\eta_{me} = 1$.
3. Increase η_{el} for more electrical power output.

3. Experimental program

The proposed wave-energy extractor in this study mainly consists of the dual coaxial cylinders and the linear generator. This section describes details of the system characteristics and instrumentations for wave-tank measurements. The tests were conducted in regular waves at the UC Berkeley Richmond Field Station Physical–Model Testing Facility, which is 68 m long, 2.44 m wide, and 1.8 m deep with a flap-type wave-maker at one end a beach on the other. To reduce the wall effects, the coaxial cylinders were placed in the centerplane of the tank and designed to have a lower resonance frequency than the first cut-off frequency of the wave tank, at which cross-mode interferences occur from the channel walls (see Ref. [17]).

3.1. Two-body cylinders

The coaxial-cylinder system as fabricated is illustrated in Fig. 3. The inner cylinder is moored to the tank bottom and is stabilized by a highly tensioned mooring cable because of the excessive buoyancy, producing about 35-kg of pretenstion in mooring cable. This stabilized inner cylinder also helps the stability of the floating outer toroidal cylinder to stay in an upright position. The outer cylinder is ballasted to meet the target resonance frequency. The relative motion between the two cylinders is made possible by the use of a pair of heave rods with linear bearings. Also, three tiny rollers were installed on the upper and lower ends of the outer cylinder circumferentially to ensure a constant gap between the two cylinders. Detailed geometric parameters of the system are listed in Table 1.

3.2. Permanent magnetic linear generator unit

The PMLG translator, consisting of the magnet array of 0.762 m long, was connected to the outer cylinder through a translator supporter, while the PMLG stator was installed with its upper part inside the inner cylinder, Fig. 3. The stator is composed of two columns of 15 teeth of 0.305 m long, and 5 adjacent teeth become one phase. A series of evaluations and performance improvements on translator and stator were detailed in Ref. [18].

This coaxial-cylinder design was to be constrained in pure heave motion, but it does not completely eliminate small undesired relative motion such as surge, pitch, and yaw. These undesired motions cause a high risk of translator and coils collapsing on each other because of the strong mutual attraction force between them. Hence, different from Ref. [18], a completely new supporting structure of the PMLG for this situation was designed and fabricated to improve the reliability and increase the stiffness of the assembly [19].

Fig. 4 shows detailed views of the stator assembly. A closed-type structure enables a magnet-coil gap width w_{gap} to be both smaller and more consistent over time. The thickness of replaceable cylindrical spacers (Fig. 5) is directly equal to the magnet-coil gap width, which makes gap width easier to control. A supporting structure for the translator is shown on the left of Fig. 5. It decouples the heave motion from all other undesired motions by the use of a horizontal slider and a ball joint that allows three degrees of freedom of rotation and two translations perpendicular to the vertical direction.

3.3. Measurements taken

To investigate the motion response of the floater, the relative displacement between the two cylinders was measured using a string potentiometer. The wave-exciting force between the two cylinders was also measured with a strain gauge force block, with

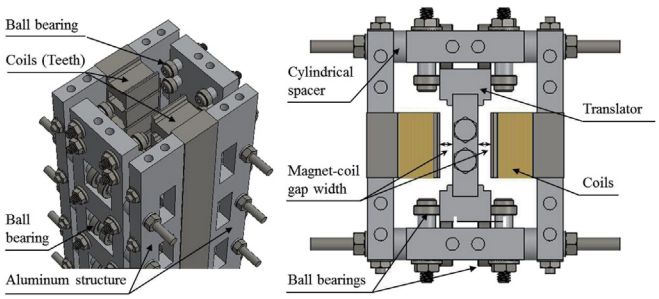

Fig. 4. Close-view of stator assembly and top-view of stator-translator assembly.

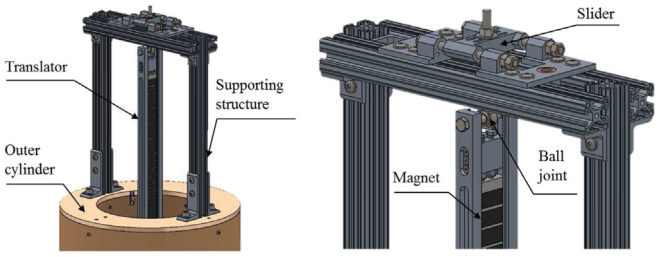

Fig. 5. Far-view and close-view of translator structure.

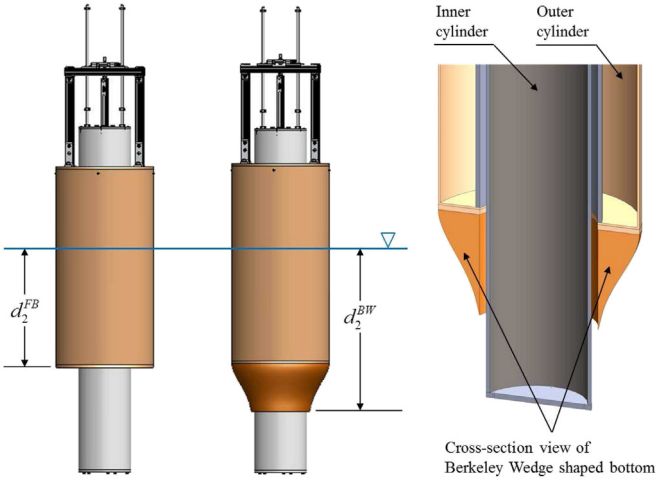

Fig. 6. Flat-versus the Berkeley-Wedge [13] bottom shape of the floater.

the outer cylinder being restricted in heave motion.

Incident wave height was measured using capacitive wave gauge, positioned at 10 m ahead of the coaxial-cylinder. Incident wave amplitude of 5.08 cm with various frequencies was applied during the experiments. It is, however, reduced by about half for the new bottom shape generating amplified motion response so that the translator always overlaps with coils. All data were collected at 200 Hz.

As the translator moves with the outer cylinder because of the incident-waves, an electric current is induced in the stator. Each phase of the stator was connected to a variable load resistor in which the energy is absorbed or dissipated. The three phases of the output were connected in a Y-winding. The voltage drop across the load resistor was measured.

4. Experimental results and validations

As discussed in Section 2, there are several ways to enhance the performance of the system with respect to energy capture. This section continues investigation on the floater and the linear generator to optimize the system performance as a energy extractor. After that, the measured performance of the coupled system will be compared to the theoretical predictions and discussed.

Table 2
Draft adjustment for Berkeley Wedge bottom shape.

Outer cylinder draft, Flat Bottom	d_2^{FB}	[m]	0.635
Outer cylinder draft, Berkeley Wedge	d_2^{BW}	[m]	0.845
Berkeley Wedge shape height		[m]	0.235
Berkeley Wedge shape weight		[kg]	15.65

Table 3
Non-dimensional hydrodynamic coefficient and determined correction factor from free-decay tests at resonance frequency.

	$\overline{\lambda}_{33}$	$\overline{\lambda}_T$	f_{vis}	$\overline{\mu}_{33}$	$\overline{\mu}_{33,exp}$	q
FB	0.029	0.245	8.448	0.254	0.347	1.366
BW	–	0.080	2.753	–	0.147	0.578

4.1. Modification of the bottom shape of floater

The flat bottom (FB) shape of the floater causes a significant separation losses in the fluid and its energy cannot be recovered [11]. To reduce viscosity effects, a special geometry of a highly asymmetrical, needle-like curved surface for one side and flat for the other side, following the so-called Berkeley Wedge (BW) was adopted. This was found to have minimal effects of viscosity recently by Ref. [13]. Fig. 6 shows Berkeley Wedge design as a shape smoother at the bottom of the floater. The draft of the modified floater was adjusted to produce the same resonance frequency as that for the flat-bottom floater, see Table 2. This new shape will amplify the floater motion and thus will increase power extraction as expected from Eqn. (20).

To investigate the viscous effect of the floater bottom shape on the performance, free-decay tests were carried out without the PMLG. The total hydrodynamic damping $\overline{\lambda}_T$ is determined using the logarithmic decrement method at resonance frequency. As a result of the bottom shape modification, the total damping of the floater significantly decreased by 67%. Also, the experimental added mass $\overline{\mu}_{33,exp}$ at resonance frequency was calculated from the resonance condition expression in Eqn. (8). In order to better predict the performance, the experimentally determined correction factors on the damping, $f_{vis} = \overline{\lambda}_T/\overline{\lambda}_{33}$, and on the added mass, $q = \overline{\mu}_{33,exp}/\overline{\mu}_{33}$, were integrated into the analytical solutions that were derived for the flat bottom in Ref. [5], see Table 3.

The measured non-dimensional wave-exciting force magnitude $|\overline{X}_3|$ of the outer cylinder relative to the incident waves is presented with the theoretical predictions from Ref. [5] in Fig. 7. Interestingly, and remarkably, these measurements show that there is no significant difference between the two different bottom shapes, over the frequency range shown. A comparison with the theoretical predictions establishes that Haskind's relation can be applied to

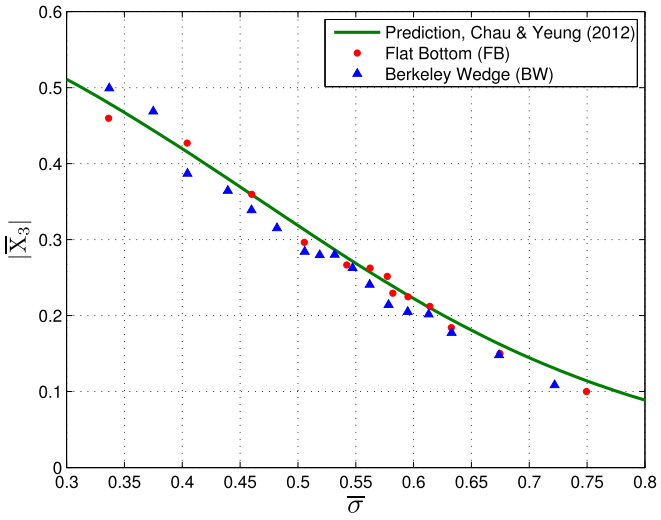

Fig. 7. Predicted and measured non-dimensional wave-exciting force.

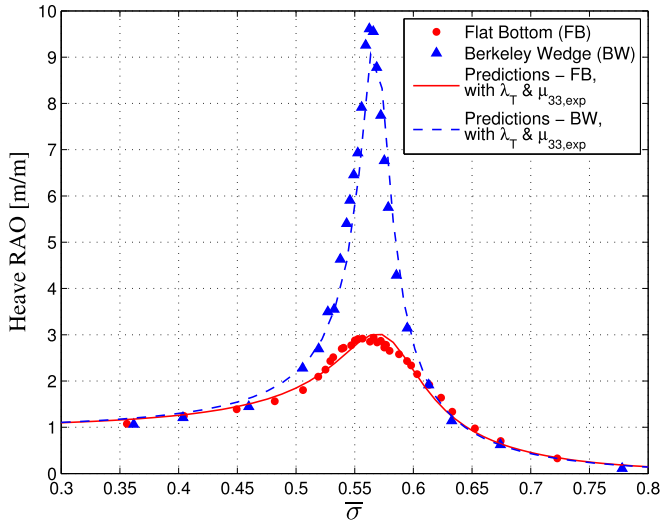

Fig. 8. Predicted and measured free motion heave RAO of the floater. Incident wave amplitude for the FB shape is 5.08 cm and 1.78 cm for the BW shape.

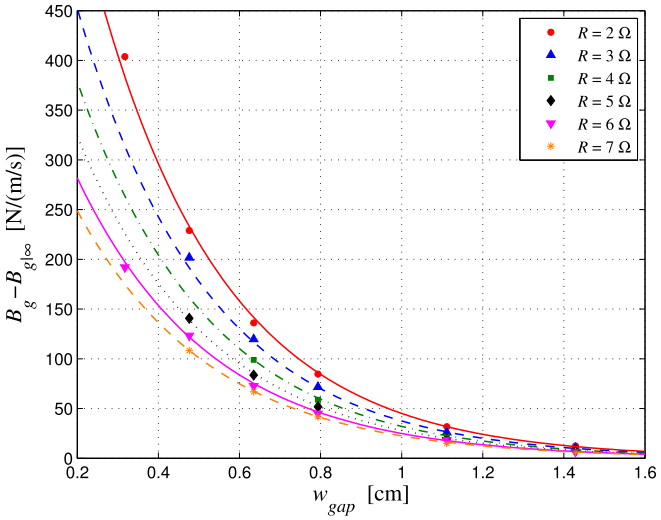

Fig. 10. Experimental $B_g - B_{g|\infty}$ values as a function of magnet-coil gap width w_{gap} and exponential fitting. Symbols are measurements and lines are empirical fitting.

both cases.

The floater motion response in free-decay for both types of bottom shapes without the PMLG, $B_g = 0$, is shown in Fig. 8. It yields an experimental non-dimensional resonance frequency $\overline{\sigma}$ of 0.567, that is a wave period of about 1.8 s. The Berkeley Wedge bottom led to a 3 times increase in motion response, as a result of the reduction of viscous damping f_{vis}. Predictions from the theoretical results of [5], with use of the correction factors of f_{vis} and q at resonance frequency, agree well with the measurements for both bottom shapes.

4.2. Performance characterization of the linear generator

The linear generator damping B_g can be controlled by changing the magnet-coil gap width w_{gap} and the connected load resistance R. Prior to coupling the PMLG unit with the coaxial cylinders, a dry-bench test was set up to evaluate its behavior. In order to determine the generator damping and electrical conversion efficiency η_{el}, both

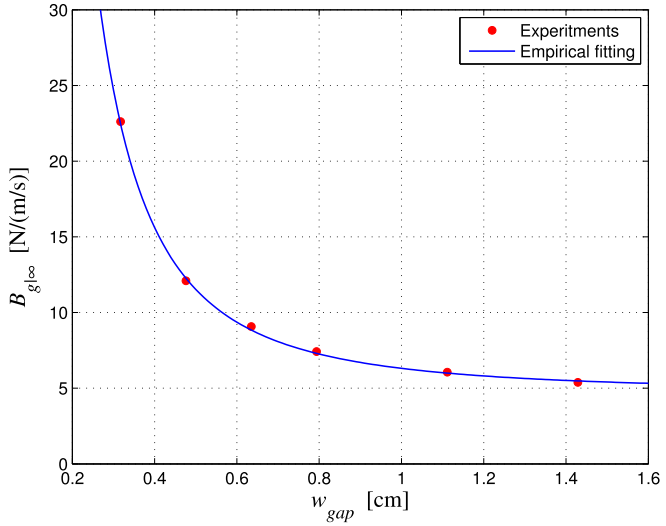

Fig. 9. Infinite-resistance (open circuit) generator damping $B_{g|\infty}$ as a function of magnet-coil gap width w_{gap} with empirical fitting.

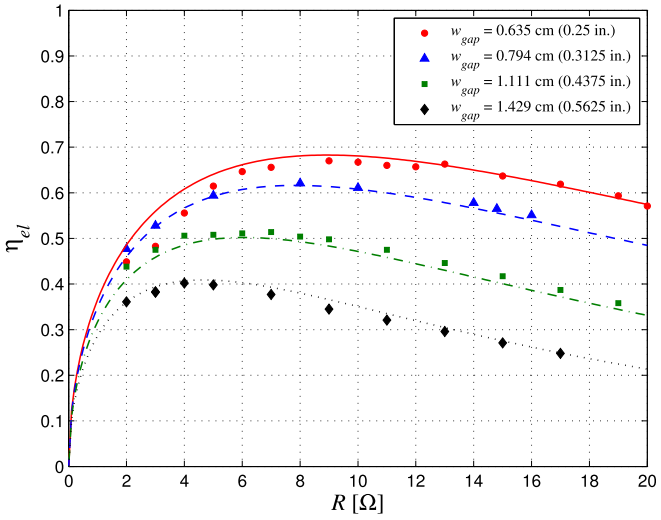

Fig. 11. Electrical efficiency η_{el} of the PMLG as a function of load resistance R and empirically-fitted curves. Symbols are measurements from dry- and wet-bench tests, and curves are the empirical fits.

the magnet-coil gap width and the connected load resistance were varied.

In open circuit, the infinite resistance damping $B_{g|\infty}$, which only depends on w_{gap}, was obtained. It includes the residual electro-magnetic damping related to cogging, eddy current losses, and bearing friction. Fig. 9 shows the obtained $B_{g|\infty}$ at the resonance frequency, and an appropriate empirical fitting form[2] was chosen as:

$$B_{g|\infty}(w_{gap}) = \alpha + \frac{\beta}{(w_{gap}/\gamma)^n} \tag{21}$$

Each series of experimental values of $B_g - B_{g|\infty}$ as a function of the w_{gap} was very well fitted by an exponential function of w_{gap} for

[2] $\alpha = 4.74$ N/(m/s), $\beta = 0.65$ N/(m/s), $\gamma = 1.52$ cm, $n = 2.11$.

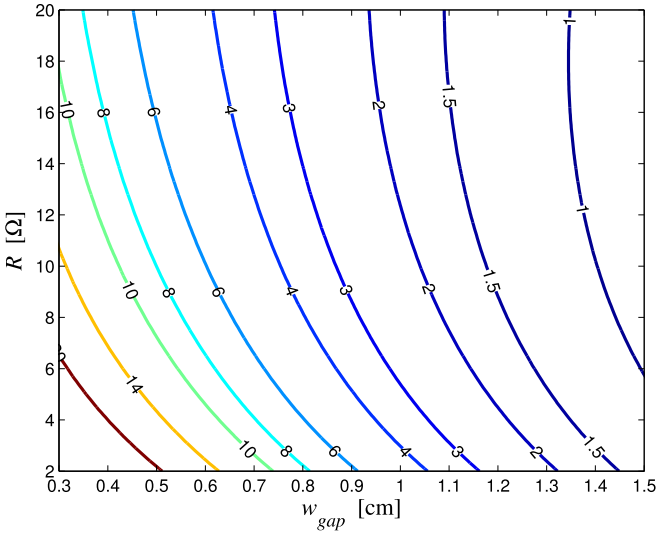

Fig. 12. Contour plot of $\tilde{f}$ for the BW from empirical expression of B_g.

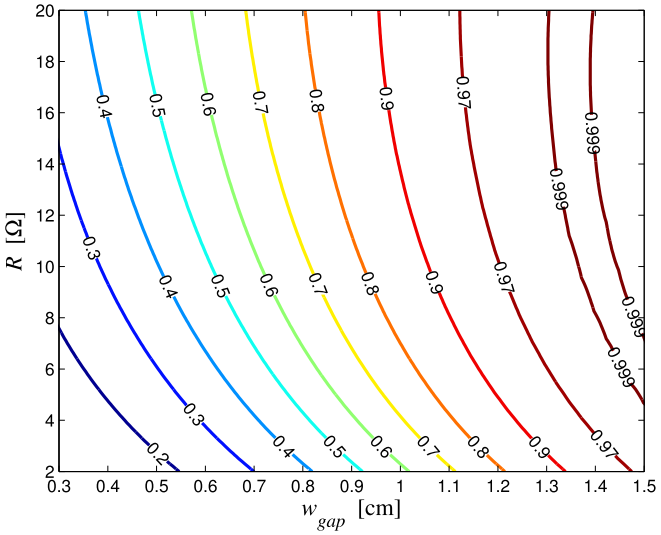

Fig. 13. Contour plot of mechanical efficiency η_{me} for the BW shaped floater using empirical fit of B_g.

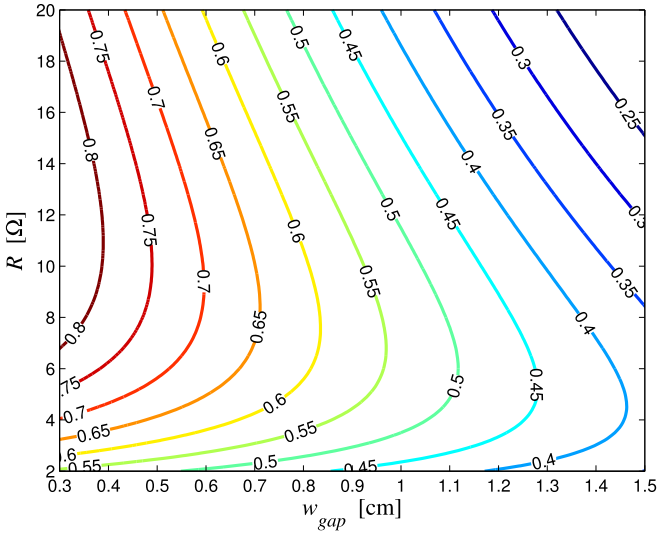

Fig. 14. Contour plot of electrical efficiency η_{el} using empirical fit.

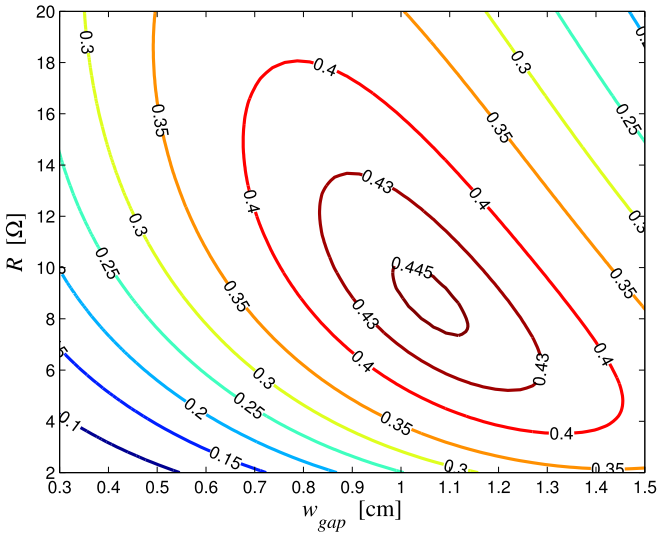

Fig. 15. Contour plot of $\eta_{el}\eta_{me}$ for the BW-shaped floater.

the different R, as it is shown in Fig. 10. The exponential fitting function[3] follows the form of:

$$B_g(R, w_{gap}) - B_{g|\infty}(w_{gap}) = A(R)e^{-B(R)\cdot w_{gap}} \tag{22}$$

Then, an empirical form for the total generator damping $B_g(R,w_{gap})$ is obtained from the above two fits:

$$B_g(R, w_{gap}) = A(R)e^{-B(R)\cdot w_{gap}} + \left[\alpha + \frac{\beta}{(w_{gap}/\gamma)^n}\right] \tag{23}$$

During the experiments, the mechanical to electrical conversion efficiency η_{el} was also measured. The results of these measurements are shown in Fig. 11, where results from the dry-bench test and the wave-tank test were displayed together. It is clear that for each value of w_{gap}, there is a specific value of R that maximizes the electrical efficiency. These results can provide some guidelines to select the best operating settings (R,w_{gap}) when the useful electrical energy output is considered. For mechanical to electrical conversion efficiency, a possible empirical formula is[4]:

$$\eta_{el}(R, w_{gap}) = \frac{A(w_{gap})\cdot R^n}{\left[R + C(w_{gap})\right]^m} \tag{24}$$

4.3. Optimal operating conditions of the coupled system

It is desired to achieve $\tilde{f} = 1$ to maximize the defined mechanical efficiency η_{me} discussed earlier. From the experimentally

[3] $A(R) = 47.02 + 27747.03/(R + 5.19)^{1.69}$ N/(m/s), $B(R) = -0.0005R^2 - 0.02R + 3.18$ cm^{-1}, R in ohms.

[4] $A(w_{gap}) = (1.03e^{-0.65w_{gap}})(15.05e^{-0.82w_{gap}})^{(m-n)}\left(\frac{m}{n}\right)^m$, $C(w_{gap}) = \left(\frac{m-n}{n}\right)15.05e^{-0.82w_{gap}}$, $n = 0.5$, $m = 4.0$, R in ohms, w_{gap} in cm.

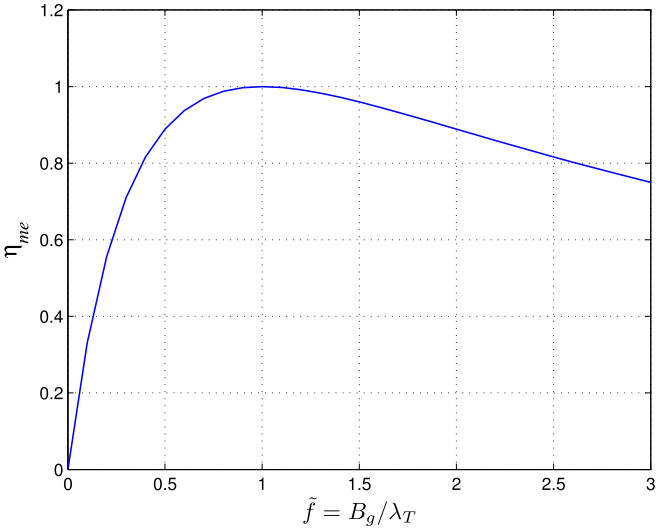

Fig. 16. Mechanical efficiency factor η_{me} as a function of $\tilde{f}$.

obtained total damping λ_T at the resonance frequency and the empirical expression, Eqn. (23), the generator damping factor $\tilde{f} = B_g(R, w_{gap})/\lambda_T$ can be calculated. Fig. 12, for example, represents the contour map of $\tilde{f}$ for the Berkeley Wedge shaped floater. It is seen that a wide range of the generator damping values is reachable with the current PMLG unit by choosing a combination of (R,w_{gap}). In the case of this Berkeley Wedge bottom, $\tilde{f}$ is obviously much higher than in the case of the flat bottom for the same (R,w_{gap}) because of the significant reduction of the total damping λ_T. Each iso-line of $\tilde{f}$ is also an iso-curve of mechanical efficiency defined in Eqn. (17), see Fig. 13.

Even though it is obvious that the capture width C_w can be maximized at exactly $\tilde{f} = 1$, in order to maximize the global efficiency of the system, or the effective capture width $C_{w|out}$, the conversion efficiency η_{el} needs to be considered. This is because the maximum effective capture width $C_{w|out}$ is equivalent to the maximum of product $\eta_{el}\eta_{me}$ from Eqn. (20), not just η_{me}. It is not necessary to maximize $\tilde{f}$ to 1. The empirically fitted electrical conversion efficiency curves in Eqn. (19) can be seen in Fig. 14. And then, from plotting of $\eta_{me}\eta_{el}$ as shown in Fig. 15, the optimal operating point of (R,w_{gap}) can be determined. In the case of the current device, the optimal operating condition, (R,w_{gap}), resulting in the highest effective capture width was determined at (11.0 Ω, 0.635 cm) for the flat bottom (FB), corresponding to $\tilde{f} = 1.58$, and (9.0 Ω, 1.11 cm) for the Berkeley Wedge (BW), corresponding to $\tilde{f} = 1.80$. Even though B_g does not exactly match λ_T, the mechanical efficiency η_{me} does not drop dramatically near $\tilde{f} = 1$ which is seen in Fig. 16, while the difference in electrical conversion efficiency is sufficiently large so that the product of the two efficiencies is higher than when $\tilde{f} = 1$.

4.4. Performance assessment of the fully coupled system

Measurements of the heave RAO for both the flat bottom and Berkeley Wedge shapes are shown, with different generator damping values of $\tilde{f}$, in Fig. 17. The RAO increases with decreasing $\tilde{f}$, or decreasing the generator damping B_g, as can be expected for both shapes. Further, the theoretical predictions with corrections of f_{vis} and q are well matched by the experimental measurements.

Fig. 18 presents the capture width $\overline{C}_w = C_w/2a_2$ non-dimensionalized by the diameter of the outer cylinder as well as the heave RAO. The measurements also match quite well with the

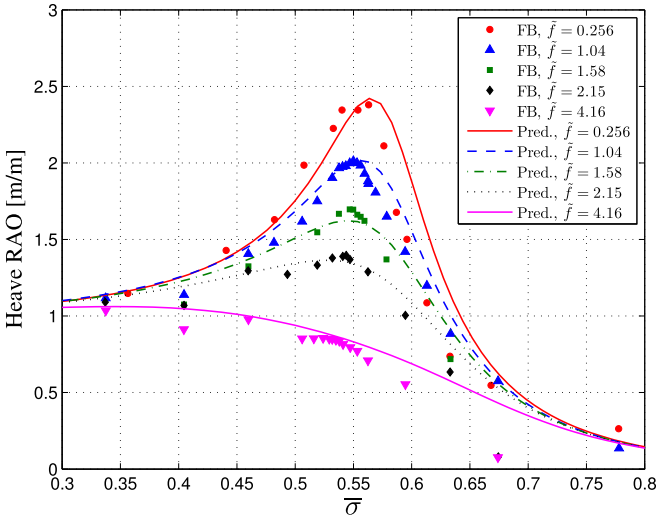

(a) RAO of the FB for a wave amplitude of 5.08 cm. $\tilde{f}$ = 0.256; (4Ω, 1.15 cm), $\tilde{f}$ = 1.04; (7.5Ω, 0.889 cm), $\tilde{f}$ = 1.58; (11Ω, 0.635 cm), $\tilde{f}$ = 2.15; (7Ω, 0.635 cm), $\tilde{f}$ = 4.16; (2.1Ω, 0.635 cm)

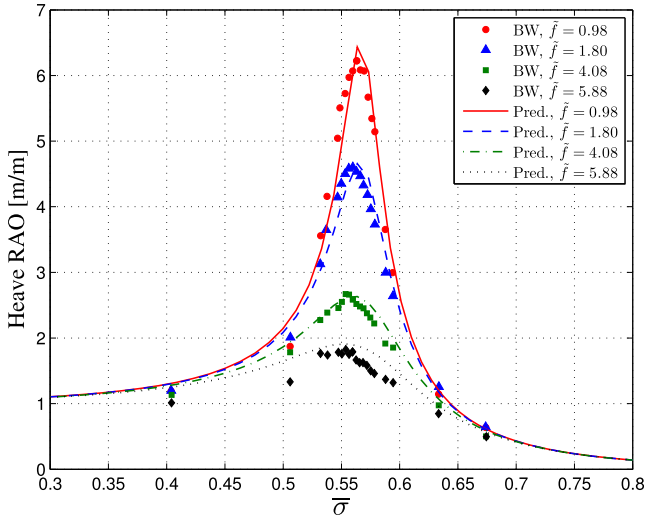

(b) RAO of the BW for a wave amplitude of 1.78 cm. $\tilde{f}$ = 0.98; (9Ω, 1.429 cm), $\tilde{f}$ = 1.80; (9Ω, 1.111 cm), $\tilde{f}$ = 4.08; (17Ω, 0.635 cm), $\tilde{f}$ = 5.88; (9Ω, 0.635 cm)

Fig. 17. Heave RAO for the FB and BW shapes.

predictions.

The RAO and capture width peak out simultaneously at the resonance frequency. The capture width is maximized for $\tilde{f} = 1$, which is expected from the earlier discussion. In terms of bottom shape optimization of the floater, the Berkeley Wedge shape led to a 3 times increase in amplitude for the same value of $\tilde{f}$ due to the much lower viscous damping, while the bandwidth is getting narrower. Other approaches such as control strategy could widen the bandwidth and thus increase the overall performance [20,21]. In the case of the highest generator force with a small magnet-coil gap and a low resistance, $\tilde{f} = 4.16$ of FB results, for example, discrepancy at high frequency is caused by the low amplitude of motion because of the highly nonlinear cogging force that becomes significant.

The non-dimensional effective capture width $\overline{C}_{w|out} = C_{w|out}/2a_2$, which accounts for the electrical conversion

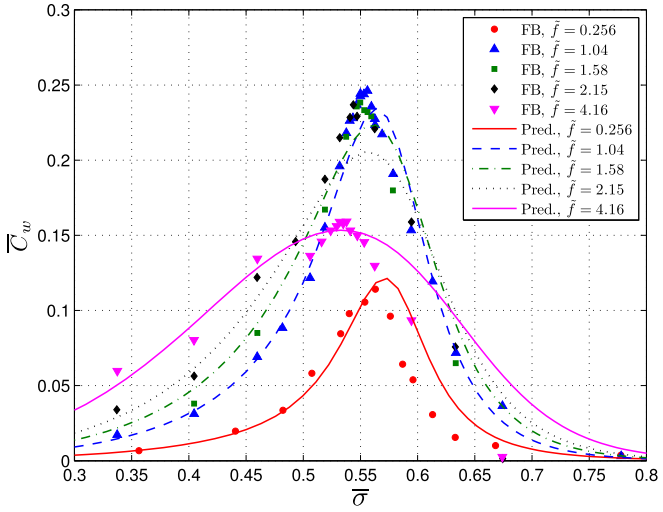

(a) C_w of the FB for a wave amplitude of 5.08 cm.
$\tilde{f}$ = 0.256; (4Ω, 1.15 cm), $\tilde{f}$ = 1.04; (7.5Ω, 0.889 cm),
$\tilde{f}$ = 1.58; (11Ω, 0.635 cm), $\tilde{f}$ = 2.15; (7Ω, 0.635 cm),
$\tilde{f}$ = 4.16; (2.1Ω, 0.635 cm)

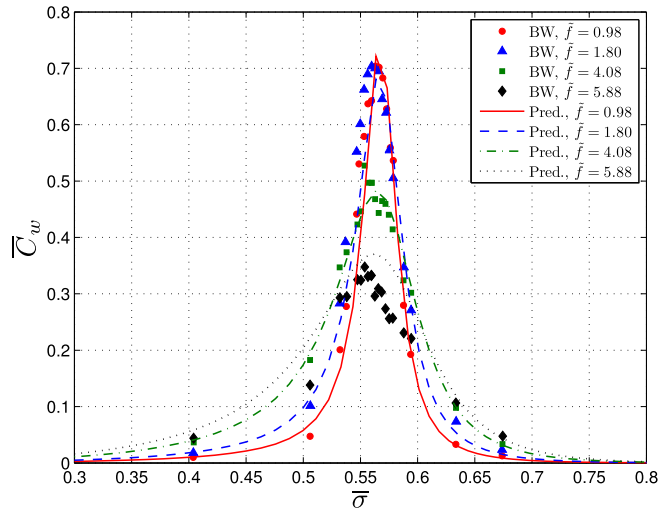

(b) C_w of the BW for a wave amplitude of 1.78 cm.
$\tilde{f}$ = 0.98; (9Ω, 1.429 cm), $\tilde{f}$ = 1.80; (9Ω, 1.111 cm),
$\tilde{f}$ = 4.08; (17Ω, 0.635 cm), $\tilde{f}$ = 5.88; (9Ω, 0.635 cm)

Fig. 18. Non-dimensional capture width for the FB and the BW shapes.

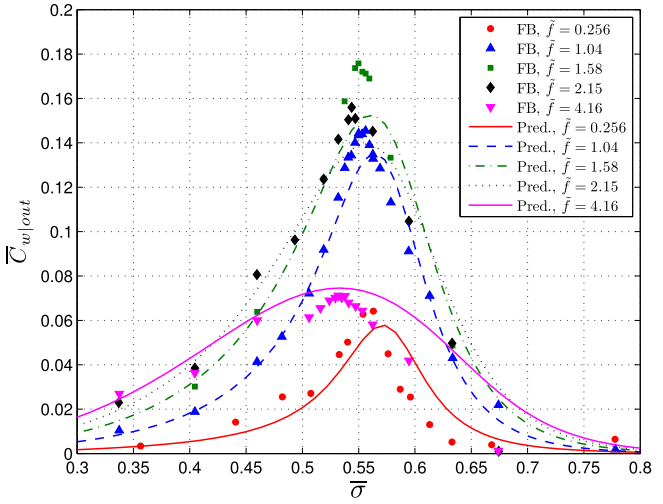

(a) $C_{w|out}$ of the FB for a wave amplitude of 5.08 cm.
$\tilde{f}$ = 0.256; (4Ω, 1.15 cm), $\tilde{f}$ = 1.04; (7.5Ω, 0.889 cm),
$\tilde{f}$ = 1.58; (11Ω, 0.635 cm), $\tilde{f}$ = 2.15; (7Ω, 0.635 cm),
$\tilde{f}$ = 4.16; (2.1Ω, 0.635 cm)

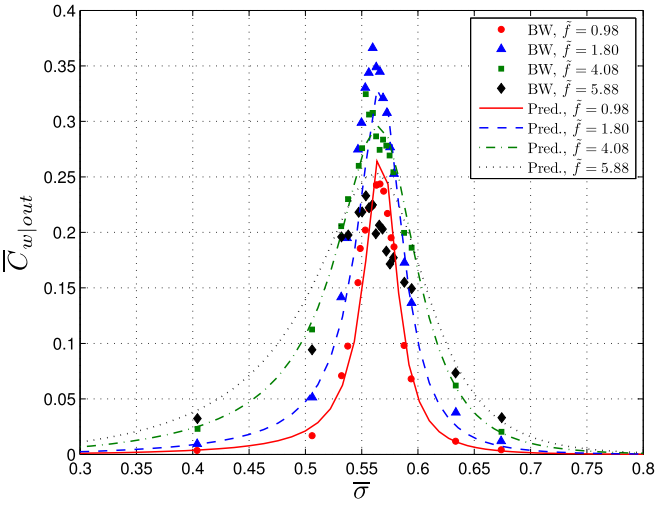

(b) $C_{w|out}$ of the BW for a wave amplitude of 1.78 cm.
$\tilde{f}$ = 0.98; (9Ω, 1.429 cm), $\tilde{f}$ = 1.80; (9Ω, 1.111 cm),
$\tilde{f}$ = 4.08; (17Ω, 0.635 cm), $\tilde{f}$ = 5.88; (9Ω, 0.635 cm)

Fig. 19. Non-dimensional effective capture width for the FB and the BW shapes.

efficiency η_{el} from the capture width results, is plotted in Fig. 19. It is demonstrated that the optimal operating point determined from $\eta_{me}\eta_{el}$ in the previous section led to the maximum effective capture width, or maximum electrical power output. Furthermore, the maximum of $\overline{C}_{w|out}$ at resonance frequency increased by a factor of 2 because of the change in the bottom shape. Numerical details on the performance optimization measured at resonance frequency are listed in Table 4.

5. Conclusions

This paper investigated the optimization the electrical-energy extraction from wave energy using a dual coaxial-cylinder system that operates with a permanent magnet linear generator.

The new floater shape adopted from the Berkeley Wedge design significantly reduced the viscous effects, hence the loss of energy to vortical fluid motion. At resonance frequency, this feature of shaping is demonstrated to lead to three times increase in the motion and the capture, compared to the flat-bottom results. Moreover, an empirically fitted formula of the PMLG unit, obtained from dry-bench test data on mechanical efficiency and electrical conversion efficiency, provided guidance for the best operating

Table 4
Experimental results of performance optimization at resonance frequency.

		$\tilde{f}$	η_{me}	$\overline{C}_w$	η_{el}	$\overline{C}_{w\|out}$
FB	max. $\overline{C}_w$	1.04	0.999	0.246	0.58	0.144
	max. $\overline{C}_{w\|out}$	1.58	0.949	0.183	0.66	0.176
BW	max. $\overline{C}_w$	0.98	0.999	0.704	0.34	0.244
	max. $\overline{C}_{w\|out}$	1.80	0.918	0.703	0.50	0.366

conditions of the generator, in terms of the take-off resistance R and generator operation gap w_{gap}, thus enabling us to maximize the useful power output from the PMLG system. As a result, the global efficiency of the system, when set at the optimal operating conditions, was about two times higher than that of the previous design.

The predictions based on inviscid linear-wave theory were modified by experimentally determined hydrodynamic coefficients to take into account viscous effects. The measurements have shown that the theoretical model was able to predict the performance of this dual coaxial-cylinder system.

Acknowledgments

We would like to thank Nils Koliha of the Technical University of Hamurg-Harburg for his initial design work, Christophe Cochet and Dr. F. P. Chau for the hydrodynamics analysis, Farshad Madhi of MML at UC-Berkeley for the data on The Berkeley Wedge, and Dr. Nathan Tom of National Renewable Energy Laboratory for his generous assistance and helpful discussions. The third author would like to acknowledge the American Bureau of Shipping for partial support that has made this research and paper possible.

References

[1] US Energy Information Administration, International Energy Outlook, 2011. Available from: http://www.eia.gov/forecasts/aeo/index.cfm [accessed March 2012].
[2] K. Gunn, C. Stock-Williams, Quantifying the global wave power resource, Renew. Energy 44 (2012) 296–304. Journal article link: http://dx.doi.org/10.1016/j.renene.2012.01.101.
[3] B. Drew, A.R. Plummer, M.N. Sahinkaya, A review of wave energy converter technology, Proc IMechE Part A: J Power Energy 223 (2009) 887–902. Journal article link: http://dx.doi.org/10.1243/09576509JPE782.
[4] A.F. de O Falcao, Wave energy utilization: a review of the technology, Renew. Sust. Energy Rev. 14 (2010) 899–918. Journal article link: http://dx.doi.org/10.1016/j.rser.2009.11.003.
[5] F.P. Chau, R.W. Yeung, Inertia, damping, and wave excitation of heaving coaxial cylinders, in: Proceedings of the 31st International Conference on Ocean, Offshore, and Arctic Engineering. OMAE2012-83987; 2012 July 1–6; Rio de Janeiro, Brazil, 2012. http://dx.doi.org/10.1115/OMAE2012-83987.
[6] E. Elwood, A. Schacher, K. Rhinefrank, J. Prudell, S. Yim, E. Amon, et al., Numerical modeling and ocean testing of a direct-drive wave energy device utilizing a permanent magnet linear generator for power take-off, in: Proceedings of the 28th International Conference on Ocean, Offshore, and Arctic Engineering. OMAE2009–79146; 2009 May 31-June 6; Honolulu, Hawaii, USA, 2009. http://dx.doi.org/10.1115/OMAE2009-79146.
[7] Ocean Power Technology. Mark 3 PowerBuoy. Available from: http://www.oceanpowertechnologies.com/mark3.html [accessed March 2012].
[8] M.J. Muliawan, Z. Gao, T. Moan, A. Babarit, Analysis of a two-body floating wave energy converter with particular focus on the effects of power take-off and mooring systems on energy capture, J. Offshore Mech. Arct. Eng. 135 (2013) 031902. Journal article link: http://dx.doi.org/10.1115/1.4023796.
[9] C. Cochet, R.W. Yeung, Dynamic analysis and configuration design of a two-component wave-energy absorber, in: Proceedings of the 31st International Conference on Ocean, Offshore, and Arctic Engineering. OMAE2012-83613; 2012 July 1–6; Rio de Janeiro, Brazil, 2012. http://dx.doi.org/10.1115/OMAE2012-83613.
[10] R.W. Yeung, A. Peiffer, N. Tom, T. Matlak, Design, analysis, and evaluation of the UC-Berkeley wave-energy extractor, J. Offshore Mech. Arct. Eng. 134 (2012) 021902. Journal article link: http://dx.doi.org/10.1115/1.4004518.
[11] N. Tom, R.W. Yeung, Performance enhancements and validations of a generic ocean-wave energy extractor, J. Offshore Mech. Arct. 135 (4) (2013) 041101. Journal article link: http://dx.doi.org/10.1115/1.4024150.
[12] R.W. Yeung, Y. Jiang, Shape effects on viscous damping and motion of heaving cylinders, J. Offshore Mech. Arct. Eng. 136 (4) (2014) 041801. Journal article link: http://dx.doi.org/10.1115/1.40276502.
[13] F Madhi, M E Sinclair, R W Yeung. The Berkeley Wedge: an Asymmetrical Energy-Capturing Floating Breakwater of High Performance. Marine Systems & Ocean Technology. J SOBENA 2014;9(1):5–16. U.S. Patent Pending, Tech ID: 23530/UC Case 2014-037-0, Link: http://techtransfer.universityofcalifornia.edu/NCD/23530.html.
[14] J.V. Wehausen, The motion of floating bodies, Annu. Rev. Fluid Mech. 3 (1971) 237–268. Journal article link: http://dx.doi.org/10.1146/annurev.fl.03.010171.001321.
[15] J. Falnes, Ocean Waves and Oscillating Systems, Cambridge University Press, 2002.
[16] R.W. Yeung, Added mass and damping of a vertical cylinder in finite-depth waters, Appl. Ocean. Res. 3 (3) (1981) 119–133. Journal article link: http://dx.doi.org/10.1016/0141-1187(81)90101-2.
[17] R.W. Yeung, S.H. Sphaier, Wave-interference effects on a truncated cylinder in a channel, J. Eng. Math. 23 (1989) 95–117. http://dx.doi.org/10.1007/BF00128863.
[18] N. Tom, Design and Control of a Coupled Permanent Magnet Linear Generator and Cylindrical Floater for Wave Energy Conversion, PhD's thesis, Department of Mechanical Engineering, University of California at Berkeley, 2013.
[19] V. Belissen, Redesign, Optimization and Fabrication of the Supporting Structure of the UC-Berkeley PMLG System for Wave Energy Extraction, Master's thesis, Department of Mechanical Engineering, University of California at Berkeley, 2014.
[20] U.A. Korde, Control system applications in wave energy conversion, in: OCEANS 2000 MTS/IEEE Conference and Exhibition.; 2000 Sep 11–14; Providence, RI, 2000. Article link: http://dx.doi.org/10.1109/OCEANS.2000.882202.
[21] N. Tom, R.W. Yeung, Nonlinear model predictive control applied to a generic ocean-wave energy extractor, J. Offshore Mech. Arct. Eng. 136 (4) (2014) 041901. Journal article link: http://dx.doi.org/10.1115/1.4027651.